International Journal of Applied Pharmaceutics

ISSN- 0975-7058 Vol 17, Issue 1, 2025

Original Article

PREPARATION AND EVALUATION OF ENTRECTINIB PLGA NANOBUBBLES BY CENTRAL COMPOSITE DESIGN

P. NANDINI, D. V. R. N. BHIKSHAPATHI*

BirTikandrajit University, Canchipur, Imphal West-795003, Manipur, India
***Corresponding author: D. V. R. N. Bhikshapathi; *Email: dbpathi71@gmail.com**

Received: 17 Mar 2024, Revised and Accepted: 18 Nov 2024

ABSTRACT

Objective: For targeted delivery of entrectinib, we created nanobubbles with a poly(lactic-co-glycolic acid) (PLGA) shell and a perfluoropentane core.

Methods: Entrectinib was encapsulated in PLGA nanobubbles by a modified W/O/W double emulsion, solvent-diffusion-evaporation technique. Central composite design was utilized to explore how four independent factors like sonication distance (X1), amplitude (X2), time (X3), and power (X4)-affected droplet size (Y1) and polydispersity Index (PDI) (Y2).

Results: The optimal sonication distance, time, amplitude, and power were 2.41 cm; 3.61 min, 44.42%, and 77.35 W. Drug-loaded nanobubbles showed a PDI of 0.196±0.005 and an average particle size of 73.53±3.08 nm, indicating a unimodal system with low PDI high zeta potential indicate formulation stability. The mean drug loading capacity was 29.27±1.54 mg/g. The remarkable drug encapsulation efficiency (82.12±2.98%) supports an inclusion complex. Transmission Electron Microscopy shows drug encapsulation does not change nanobubbles' spherical shape. Fourier-transform infrared spectroscopy and Differential scanning calorimetry revealed nanobubble-drug complex production. Nanobubbles emitted more entrectinib than the solution. Drug release via ultrasound was different. At 6 h, sonication released 46.08% of entrectinib and 26.42% without. Entrectinib released 99.34% after 24 h versus 58.93% without ultrasonography. The formulation's consistent size distribution remained stable after 180 days. Parenteral safety and non-toxicity were shown by these nanobubbles at 15 mg/ml. *In vitro* ultrasonic increases cell uptake. The viability of MCF-7 cells was assessed following exposure to entrectinib at 10 to 120 µM dosages. All entrectinib formulations showed little cytotoxicity, up to 98% cell survival at 10 µM doses.

Conclusion: PLGA nanobubbles can be used in ultrasound-responsive formulations to deliver targeted drugs to fight cancer and other diseases.

Keywords: Entrectinib, Cancer, Solvent-diffusion-evaporation technique, Central composite design, Nanobubbles, Ultrasound-assisted medication, Cytotoxicity

DOI: https://dx.doi.org/10.22159/ijap.2025v17i1.50891 Journal homepage: https://innovareacademics.in/journals/index.php/ijap

INTRODUCTION

Entrectinib, marketed as Rozlytrek™ is a pharmaceutical breakthrough that inhibits important tyrosine receptor kinases (TRKA, TRKB, and TRKC), ROS1, and anaplastic lymphoma kinases (ALK), revolutionizing cancer treatment. Overexpression and constitutive activation of these kinases in cancer cells are common [1-4]. Its unique ability to suppress brain tumor growth makes it a promising brain tumor treatment [5]. This favourable profile makes entrectinib a prominent oncology player, promising better cancer treatment outcomes. Entrectinib was recommended at 600 mg/d for adults and 300 mg/m^2 for children 12 and older [6, 7]. Entrectinib, a class II Biopharmaceutics Classification System drug, has unique pharmacokinetic features that affect its bioavailability and clinical efficacy and it is lipophilic and basic, resulting in modest permeability [8-10]. Entrectinib looks promising for treating advanced solid tumors with gene fusions or mutations [11]. To achieve consistent therapy outcomes for solid tumor patients, these formulations should improve solubility, bioavailability, and dosage [12]. The salt formation, co-solvency, micronization, complexation, and permeation enhancers have been used to improve solubility and bioavailability, but these systems have limited drug delivery efficacy, requiring more novel approaches [13, 14]. Nano-based Drug Delivery Systems (NBDDS) have received attention because they could revolutionize poorly soluble medication delivery and bioavailability [15, 16].

Entrectinib nanoparticles could be encapsulated in biodegradable polymers like PLGA or PEG to improve solubility and stability [17]. While Entrectinib nanoparticles development is still early, NBDDS may help improve its solubility and bioavailability and improve its cancer treatment efficacy [18]. Compared to other nano-delivery systems, nanobubble technology may offer versatile drug administration, controlled release, nontoxic, biocompatible, improved biological barrier penetration, and increased imaging. Its unique features make it a versatile and effective drug delivery platform [19, 20]. Nanobubbles also increase tumor drug delivery, which is problematic with existing techniques [21]. PLGA is biodegradable, biocompatible polymer and is frequently utilized in medication delivery and biomedicine [22, 23]. Adjusting fabrication parameters like the polymer-surfactant ratio, sonication time, and drug concentration can optimize PLGA nanobubble composition. Therefore, the best composition of PLGA nanobubbles can be achieved by modifying these parameters to achieve the appropriate size, stability, and drug-loading efficiency for the intended application [24-26].

MATERIALS AND METHODS

Materials

Entrectinib was gifted from Aelida Pharmaceuticals in Haryana, India. Cell culture media, trypsin, PLGA, and newborn calf serum were all purchased from Sigma Aldrich Chemicals Private Limited in Bangalore, India. Dichloromethane and perfluoropentane were supplied by S.D. Fine Chem. Pvt. Ltd. of Mumbai, India. Only Milli-Q water, manufactured by Millipore, was used in the study. Analytical-grade reagents and materials were utilized throughout the experiment.

Methods

Preparation of PLGA nanobubbles encapsulating entrectinib

Entrectinib was encapsulated in PLGA nanobubbles using a customized W/O/W double emulsion, solvent-diffusion-evaporation method [27]. Around 900 mg PLGA was dissolved in 10 ml dichloromethane and combined with 90 mg entrectinib under sonication. Primary emulsion was formed by emulsifying this combination with a digital Sonifier® SFX150 (Branson Ultrasonic,

Danbury, USA) in an ice bath under optimum circumstances. The initial emulsion was immediately poured into a 20 ml 1% w/v PVA solution. Ultrasonic probe treatment at 30 W for 1 minute in darkness formed a double emulsion. After gently adding the emulsion to a 100 ml isopropanol solution (5% v/v), it was agitated at 2000 rpm for 5 h at room temperature to extract dichloromethane. The mixture was centrifuged for 10 min at 12,000 rpm. Centrifuged supernatant was removed, and the precipitate was carefully washed with deionized water. Centrifugation and washing were done three times. Washed nanobubbles were freeze-dried in the dark for 36 h using LYPH LOCK 4.5 (Labconco Corporation, Kansas City, MO). C3F8 gas was injected into the lyophilization chamber at 50 ml/min for 1 minute through a specific vial connector. Screw vials were sealed. Entrectinib was encapsulated in PLGA nanobubbles after this rigorous process, ready for use.

Optimization of ultrasound parameters using RSM

DOEs

The optimization of ultrasonic processes heavily relies on Response Surface Methodology (RSM) because of its exceptional capacity to match mathematical models. The use of RSM, a mathematical and statistical method, is crucial here since it paves the way for the development of prediction models that detail the association between various factors and the intended results of ultrasonic procedures. Applying RSM allows for the thorough collection and modelling of nonlinearities and complex interactions within the system, which in turn allows for accurate optimization for improved efficiency and results in ultrasonic-based applications [28].

The operating parameters for ultrasound, as established in the first experiments, included a sonication distance (the distance from the base of the vessel to the probe) of 2.0 to 3.0 cm, a sonication time of 3 to 4 min, amplitude of 40 to 50%, and a power of 80 to 90 W. During the sonication process, the containers were placed in an ice water bath and a 5-second time interval was used. After sonication, the samples were kept in a dark, cool place (25 °C). To determine how each variable affected particle size (PS) and polydispersity index (PDI), CCD was used to evaluate sonication distance (A), amplitude (B), time (C), and power (D). The design incorporates a factorial design at two levels (typically -1 and +1), center points for experimental errors, and axial points for response surface curvature. This design generally varies factors (independent variables) at three levels: low (-1), center (0), and high (+1). To assess experimental error and curvature, center points (0) are duplicated. Axial points (-α and+α) are used to evaluate response surface curvature. Fitting a second-order polynomial equation (equation 1) permits the modelling and optimization of the response variable based on the factors. A CCD with four elements has a general second-order polynomial equation:

$$Y = \beta_0 + \sum_{i=1}^{4} \beta_i X_i + \sum_{i=1}^{4} \beta_{ii} X_{ii}^2 + \sum_{i<j}^{4} \beta_{ij} X_i X_j + \varepsilon$$

Where:

Y is the predicted response variable.

β_0-is the model intercept.

β_i-are the linear coefficients representing the effect of each factor.

β_{ii}-are the quadratic coefficients representing the effect of each factor squared.

β_{ij}-are the interaction coefficients representing the effect of interactions between different factors.

X_i and X_j are the levels of the independent variables (factors).

ε is the error term.

CCD experimental data is used to estimate equation terms using regression analysis. The predictor polynomial equation models response variable behaviour based on factors and their interactions using the coefficients ($\beta_0, \beta_i, \beta_{ii}$, and β_{ij}). Detailed preliminary trials determined the particularly selected components and their values (table 1). A structured design was used to conduct the studies, and table 2 shows the dependent variable outcomes. Design-Expert (Stat-Ease V13.0.5.0) was then used to analyze the response surfaces within the experimental range.

Table 1: Different levels of independent variables and goal of dependent variables

Independent factors	Levels				
	-α	-1	0	+1	+α
A – Sonication distance (cm)	1.79	2.0	2.5	3.0	3.20
B – Sonication time (min)	2.79	3	3.5	4	4.20
C – Sonication amplitude (%)	32.93	35	40	45	47.07
D – Sonication power (W)	65.86	70	80	90	94.14
Dependent variables	Goal				
Y1-Droplet size (nm)	Decrease				
Y2 – PDI	Decrease				

Data analysis

To investigate variable correlations, a complete statistical analysis was done after the experiments. Many models described these linkages. Statistical factors such as model p-value, lack of fit p-value, regression coefficient (R^2), adjusted R^2, and coefficient of variation were assessed to determine the best-fitting model. To help choose the most relevant and efficient model, model terms with p-values over 0.005 are usually considered irrelevant and can be eliminated. To improve our regression equation, we used backward elimination to remove independent variables that did not significantly contribute. This strategy required carefully eliminating non-contributing elements one by one. We used three-dimensional response surface plots to understand the link between selected response parameters and two independent variables. These plots showed functional linkages, illuminating the complex dynamics. To further visualize independent variables' effects on response parameters, we used perturbation and contour plots. Graphical representations helped us understand variable effects, deepening our analysis [29].

Optimization approach and verification

By constraining response parameters and influential factors, we found the ideal independent variable values via numerical optimization. These limitations helped optimize for desired results [30]. Next, the nanoformulation was carefully manufactured in triplicate under ideal conditions. This method supported the efficacy and dependability of the optimization strategy, confirming that the optimal points produced the intended and consistent formulation results.

Characterization of prepared entrectinib nanobubbles

PS, PDI, and zeta potential (ZP)

Entrectinib nanobubbles PS distribution was determined using dynamic light scattering (DLS). Every sample was measured at 90°. We diluted the samples with Milli-Q water before measuring. Cumulated analysis using three measurements determined the particles' mean hydrodynamic diameter (Dh) and PDI with an additional electrode, the same equipment measured ZP. Experiments were conducted in triplicate at 25±2 °C.

Table 2: Experiments as per the design and outcomes for the dependent variables

Expt	A	B	C	D	Y1	Y2
1	2.5	4.20	40	80	96.75	0.192
2	3	3	35	90	204.78	0.256
3	3	4	35	70	223.43	0.264
4	3	3	35	70	253.23	0.284
5	3	4	45	90	101.56	0.274
6	3.20	3.5	40	80	157.73	0.262
7	3	3	45	70	152.53	0.232
8	2.5	3.5	40	80	89.13	0.188
9	2.5	3.5	40	65.86	129.82	0.227
10	2.5	3.5	47.07	80	97.12	0.204
11	2.5	2.79	40	80	118.29	0.192
12	2	3	35	90	188.76	0.232
13	2	4	35	90	164.12	0.227
14	2.5	3.5	40	94.14	61.22	0.252
15	2.5	3.5	40	80	95.98	0.192
16	2.5	3.5	32.93	80	230.89	0.214
17	1.79	3.5	40	80	136.62	0.224
18	2	3	35	70	234.54	0.265
19	2	3	45	90	85.76	0.251
20	2	4	45	70	122.38	0.198
21	3	4	35	90	187.54	0.238
22	2.5	3.5	40	80	100.23	0.186
23	2.5	3.5	40	80	90.36	0.183
24	2.5	3.5	40	80	94.28	0.179
25	2	3	45	70	126.77	0.206
26	3	4	45	70	140.54	0.212
27	3	3	45	90	105.18	0.273
28	2	4	35	70	206.43	0.232
29	2	4	45	90	87.12	0.275
30	2.5	3.5	40	80	84.17	0.202

Drug payload and encapsulation efficiency (EE)

The percentage of entrectinib encapsulated from the nanobubbles preparation amount is called EE. The drug's weight proportion in the nanobubble formulation is its payload [31]. To assess the amount of entrectinib in the formulation, a weighed quantity was dissolved in dichloromethane, sonicated for 10 min to break down the complex, diluted, and analyzed using a UV spectrophotometer at 262 nm. The "percent drug payload" and "percent drug EE" were estimated using below equations:

$$\%\ Drug\ pay\ load = \frac{Weight\ of\ drug\ encapsulated\ in\ nanoformulation}{Weight\ of\ the\ NS\ formulation\ taken\ for\ analysis} \times 100$$

$$\%\ Drug\ encapsulation\ efficiency = \frac{Weight\ of\ drug\ encapsulated\ in\ nanoformulation}{Initial\ weight\ of\ the\ drug\ fed\ for\ loading} \times 100$$

Transmission electron microscopy (TEM)

TEM evaluated entrectinib-loaded and plain nanobubble morphology. A film-coated copper grid was stained with a 2% (w/v) phosphotungstic acid solution after a drop of diluted nanoparticle suspension. Drying the sample enhanced contrast. The analysis was done at 25,000× magnification.

Fourier-transformed infrared (FTIR) spectroscopy and differential scanning calorimetry (DSC)

A Tensor 27 FTIR Spectrophotometer was used to obtain potassium bromide disc FTIR spectra of entrectinib, plain nanobubbles, and entrectinib-loaded nanobubbles. Analysis was conducted in the 4000 to 600 cm^{-1} spectral range. The Perkin Elmer DSC/7 differential scanning calorimeter with a TAC 7/DX instrument controller was used to analyze entrectinib, plain nanobubbles, and entrectinib-loaded nanobubbles. The melting point and heat of fusion were calibrated with indium. In conventional aluminum pans, the samples were heated at 10 °C/min from 30-400 °C under a nitrogen purge. Analysis of 5 mg samples was done three times.

***In vitro* drug release study and kinetics analysis**

At 37 °C, dialysis bags were used to measure entrectinib release from nanobubbles *in vitro*. The release was monitored for 24 h using a dialysis bag with a 12-14 kDa molecular weight limit. Predetermined intervals were used to replace samples with fresh phosphate buffer. We experimented three times. In drug delivery system evaluation, a drug release kinetics study reveals how and when a drug is released from a formulation. Mathematical models of drug release kinetics help explain and predict drug release.

Ultrasound stability of entrectinib nanobubbles

Ultrasound was applied to entrectinib-loaded nanobubbles at defined parameters and durations. Pre-and post-ultrasound evaluations used optical microscopy to measure nanobubble structural integrity.

Evaluation of stability of entrectinib nanobubbles

Entectinib nanobubble stability was tested for 1 mo at 4 °C, 25 °C, and 40 °C. Entrectinib content, EE, average PS, and appearance were examined regularly to assess stability.

Determination of hemolytic activity

PLGA nanobubbles were tested for hemolysis using human blood. A suspension of erythrocytes was incubated at 37 °C for 2 h with various nanobubble percentages (v/v). The centrifuged supernatant was analyzed at 543 nm [32]. A defined equation calculated the hemolysis percentage compared to 100% hemolysis control.

$$\%\ Hemolysis = \frac{ABS_{Sample} - ABS_0}{ABS_{100} - ABS_0}\ X\ 100$$

Where ABS_0 and ABS_{100} are the absorbances of the solution at 0 and 100 % hemolysis, respectively.

Cell culture

MCF-7 cells (human breast cancer cells) were obtained from The American Type Culture Collection (ATCC, Manassas, VA, USA), and Bogoo Biotech Co. Ltd. (Shanghai, China) graciously contributed to Adriamycin-resistant MCF-7/ADR cells. MCF-7/ADR cells were grown in 500 ng/ml entrectinib to adapt to drug resistance. Subculture raised entrectinib to 1000 ng/ml. Later research used these cells, which thrived and proliferated stably in a culture

medium with 1000 ng/ml entrectinib. In a humidified 5% CO_2 incubator at 37 °C, all cells were grown in RPMI 1640 with 10% FBS, 100 U/ml penicillin, and 100 mg/ml streptomycin.

Cell viability assay

The viability of MCF-7 and MCF-7/ADR cells in the presence of free entrectinib, plain nanobubbles, and entrectinib nanobubbles was measured using a cell counting kit-8. Cell suspensions of MCF-7 or MCF-7/ADR were planted at a density of 7×103 cells/well in a 96-well plate and incubated overnight at 37 °C A new culture medium was used to incubate cells with free entrectinib and nanobubbles (at doses of 5, 20, 40 µg/ml) for 72 h. Ten microliters of thawed CCK-8 solution were added to each well and incubated for 1 h before being measured at 450 nm using a microplate reader (Model 680, Bio-Rad, PA, USA). The relative cell viability was estimated as a percentage of nontreated cells.

Cellular uptake of entrectinib nanobubbles

The MCF-7 cells were sown at 1.5×104 cells/well in 48-well plates and left to attach for 24 h [33]. Replaced supernatants with fresh culture media containing entrectinib nanobubbles at 80, 160, and 240 µg/ml per well and incubated for 6 h. Another group examined time-dependent uptake. Entrectinib nanobubbles (final concentration 40 µg/ml) were treated with cells for 4, 6, and 8 h. Following incubation, all samples were washed three times with PBS and examined under a fluorescence microscope (TE-2000U, Nikon, Tokyo, Japan).

Data presentation and statistical analysis

The quantitative data was reported as mean±SEM. The investigations used One-way ANOVA and Bonferroni testing to assess differences between groups. A p-value of<0.05 was considered significant.

RESULTS AND DISCUSSION

The small size and core-shell composition of nanobubbles makes them ideal medication delivery vehicles. They are nanometer-sized and contain gases or vaporizable chemicals like perfluorocarbons. The center is stabilized by a lipid, polymer, or albumin shell. Novel nanocarriers such as nanobubbles have improved stability, drug-loading capacity, and extravasations. They may migrate from blood arteries into nearby tissues due to their small size [34]. The small size and unique physical features of polymer-shelled nanobubbles allow them to enter the extra vascular region, making them ideal for targeted medication delivery. Researchers investigated biodegradable and non-biodegradable polymers for nanobubbles. Biocompatibility and biodegradability make PLGA a popular polymer [35]. Sutures, bone implants, screws, and drug-release matrices use PLGA [36].

This study used entrectinib-specific PLGA nanobubbles. Nanobubbles were made from free carboxylic end-group PLGA polymer. Using perfluoropentane for the inner core and PLGA (50:50 ratios; intrinsic viscosity 0.22 dl/g, MW = 15000) for the shell, blank and entrectinib-loaded nanobubbles were Entrapped in the core, the drug formed nanoparticles. Variations in formulation component concentrations produced several batches of entrectinib-loaded nanobubbles. Initial investigations showed inconsistent PS distribution, stressing the importance of factors. The nanobubbles' PS and PDI were affected by the sonication distance (A) (the distance between the vessel bottom and the ultrasound probe) of 2.0 to 3.0 cm, the time (B) of 3–4 min, the amplitude (C) of 35%–45%, and the power (D) of 70–90 W. These techniques were difficult to replicate due to nanobubble preparation variations.

The quality and efficacy of entrectinib-loaded nanobubbles depend on droplet size distribution. It helps determine nanobubble formulation homogeneity and consistency, particularly medication distribution. Drug delivery applications require limited droplet size dispersion. It shows an optimized formulation procedure that produces nanobubbles with minimum size fluctuation, improving drug-loading efficiency and delivery uniformity. A wider or unequal droplet size distribution may indicate formulation or medication encapsulation issues. Thorough optimization of formulation variables including sonication distance (A), time (B), amplitude (C), and power (D) is needed to achieve the required droplet size distribution. Each of these variables affects nanobubble properties, including droplet size. Creating nanobubbles with the proper droplet size distribution for drug administration, bioavailability, and therapeutic effectiveness requires finding the right balance and combination of these parameters.

The multivariate statistical technique RSM was beneficial for formulation optimization studies in this investigation. The building of a mathematical model that visually shows the interactive effects of components within an experimental range reveals controlled variable relationships. RSM also expedites optimization based on intended outcomes**.** To optimize preparation conditions, the CCD technique was chosen for investigating quadratic response surfaces and building accurate second-order polynomial models [37]. All 'p' values were below 0.05, proving that the chosen model was very significant, notably for PS and PDI.

RSM optimization

Statistical analysis

With a four-factor, five-level CCD, 30 trials were undertaken. Table 2 shows these experiments' independent and dependent variables. Droplet size (Y1) ranged from 61.22 to 253.23 nm across all trials, whereas nanobubble PDI (Y2) was 0.179 to 0.284. We used result RSM to explore the interactions between various independent variables and find the best circumstances for the intended result. While assessing variable interactions, RSM methods reduce experimental runs. Stat-Ease Design Expert® (V13.0.5.0) program extensively analyzed the data to determine the analysis of variance (ANOVA), regression coefficients, and the regression equation. To model the results, a second-order quadratic model was fitted to the data and validated using ANOVA, lack of fit, and multiple regression coefficient (R^2) values.

As seen in tables 3 and 4, the best-fitting quadratic models had the highest F value. The variables' mathematical equations from multiple linear regression analysis are shown in table 5. The polynomial equations show how each independent variable and their combined influence affect the response variables. Independent variable coefficients show their effect on response variables. Multiple variable and higher-order coefficients indicate interaction and quadratic effects, respectively. A positive sign indicates synergy, whereas a negative sign indicates opposition. All regression equations were significant.

Table 3: ANOVA of the quadratic model for the response droplet size (Y1)

Source of variation	Sum of squares	Degrees of freedom	Mean square value	F-value	p-value prob>F
Model	84095.58	8	10511.95	641.97	<0.0001
A-Sonication distance	1670.13	1	1670.13	102.00	<0.0001
B-Sonication time	1108.44	1	1108.44	67.69	<0.0001
C-Sonication amplitude	43260.75	1	43260.75	2641.96	<0.0001
D-Sonication power	9333.15	1	9333.15	569.98	<0.0001
BC	411.58	1	411.58	25.14	<0.0001
A^2	6793.53	1	6793.53	414.89	<0.0001
B^2	440.56	1	440.56	26.91	<0.0001
C^2	11771.34	1	11771.34	718.88	<0.0001
Residual	343.86	21	16.37		
Lack of Fit	183.63	16	11.48	0.3581	0.9466
Pure Error	160.24	5	32.05		
Cor total	84439.44	29			

Table 4: ANOVA of the quadratic model for the response PDI (Y2)

Source of variation	Sum of squares	Degrees of freedom	Mean square value	F-value	p-value prob>F
Model	0.0275	6	0.0046	40.07	<0.0001
A-Sonication distance	0.0020	1	0.0020	17.63	0.0003
C-Sonication amplitude	0.0004	1	0.0004	3.63	0.0692
D-Sonication power	0.0014	1	0.0014	12.40	0.0018
CD	0.0063	1	0.0063	54.95	<0.0001
A^2	0.0070	1	0.0070	60.87	<0.0001
D^2	0.0061	1	0.0061	53.06	<0.0001
Residual	0.0026	23	0.0001		
Lack of Fit	0.0023	18	0.0001	1.99	0.2287
Pure Error	0.0003	5	0.0001		
Cor Total	0.0301	29			

Table 5: Regression equations for both the responses

Dependent variable	Regression equation
Y1	93.31+9.14 A– 7.44 B – 46.51 C – 21.60 D+5.07 BC+26.60 A^2+6.77 B^2+35.02 C^2
Y2	0.1932+0.0100 A-0.0046 C+0.0084 D+0.0198 CD+0.0264 A^2+0.0246D^2

Besides coefficients, the lack of fit value is an important statistical measure for model fitness assessment. A comparison of residual error and pure error from replicated center points achieves this. Significant fit value loss indicates poor prediction efficiency. A model with a non-significant lack of fit is crucial. A non-significant lack of fit in both quadratic models confirmed model fit. Key parameters like R^2 value, adjusted R^2 value, and coefficient of variation summarise multiple linear regression analysis results for all models. R^2 shows variation around the mean. Both response variable R^2 values were over 0.91, indicating that the selected models explained experiment behaviour. In addition, the adjusted R^2 value is crucial to model adequacy. The amount of variable terms in the model can increase R^2 values, which does not necessarily indicate model soundness. Therefore, the modified R^2 value is a better model adequacy indicator. Droplet size and PDIR^2 values were 0.9959 and 0.9127, respectively. Both models had consistent R^2 values and adjusted R^2 values, indicating that non-significant factors had been excluded. The coefficient of variance for both replies was 2.91 and 4.71, proving the data' repeatability and dependability. These criteria emphasize experimental stability and consistency, bolstering the study's credibility. The projected values and experimental data coincide well in fig. 1. For all three responses, data points are linked to anticipated values. These pictures show that both models identified the process and formulation variables needed to make entrectinib nanobubbles. The close match between expected and actual findings shows that the existing models accurately and reliably capture the nanobubble preparation process.

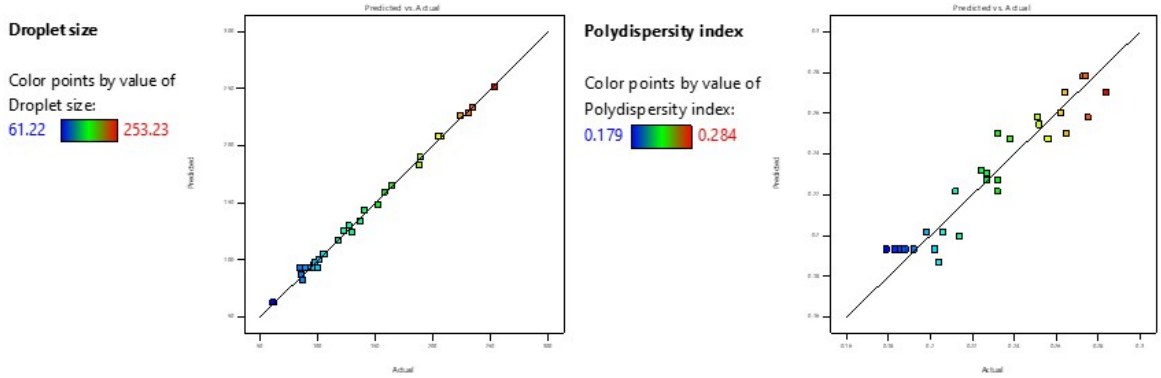

Fig. 1: Comparison between predicted and actual values of droplet size and PDI droplet size (Y1)

To manage nanobubble quality, droplet size must be measured because PS affects physical attributes and stability. Nanocarrier size affects tumor tissue and organ penetration and retention [38]. Table 2 showed nanobubble PS from 61.22 to 253.23 nm. The polynomial model showed that all factors (A, B, C, and D) affected nanobubble PS. The quadratic droplet size model had a substantial F-value of 641.97. Individual factors (A, B, C, and D), interaction term BC, and quadratic terms (A^2, B^2, and C^2) significantly affected droplet size (p-values<0.0500). "Lack of Fit F-value" (0.36) indicated little significance. Models with non-significant misfits fit well. The factorial equation for droplet size showed that C had a greater impact than D, B, and A, with R^2 and adjusted R^2 values of 0.9959 and 0.9944, respectively. The observed values matched the projected values. Perturbation, 3D-surface, and contour plots were used to show how independent variables affect droplet size. In the perturbation plot, A, B, C, and D affected droplet size individually. Fig. 2 indicated that C had the greatest impact on droplet size, followed by D and A and weakly by B. 3D response surface and contour plots showed independent variable interaction and quadratic effects. The interaction effect of B and C (CD) at a constant A and D on droplet size is shown in fig. 2.

PDI

Nanobubble droplet size affects its physical qualities and stability, making it an important quality control metric. Nanocarrier size has a major impact on tumor tissue and organ penetration and retention [38]. Table 2 shows nanobubble PS that ranged from 61.22 to 253.23 nm. According to the polynomial model, all factors (A, B, C, and D) affected nanobubble PS. An F-value of 641.97 showed that the droplet size quadratic model was significant. Each variable (A, B, C, and D), the interaction term BC, and the quadratic terms A^2, B^2, and C^2 significantly affected droplet size, with p-values below 0.0500. The "Lack of Fit F-value" showed no significance (0.36). A well-fitting model has no major misfit. In the droplet size factorial equation, C had

a greater impact than D, B, and A, with a strong correlation coefficient (R^2) and adjusted R^2 values of 0.9959 and 0.9944 from the model. The observed values matched the projected values. Perturbation, 3D-surface, and contour plots explored the main and interacting impacts of independent variables on droplet size. According to the perturbation plot, A, B, C, and D affect droplet size. According to fig. 3, C had the greatest impact on droplet size, followed by D and A, and B had little. 3D response surfaces and contour plots showed independent variable interaction and quadratic effects. In fig. 3, B and C (CD) interact to affect droplet size at a constant A and D.

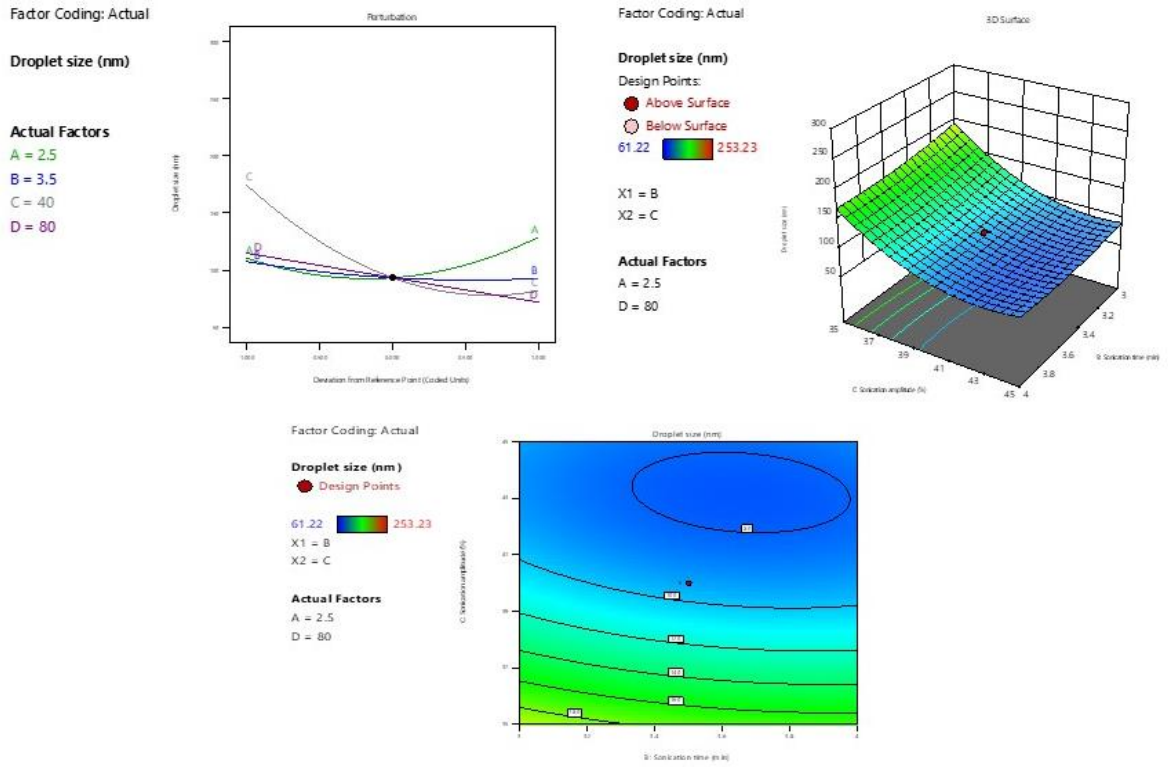

Fig. 2: Two-dimensional perturbation, 3D-RSM and contour plot– effect of A, B, C, and D on droplet size

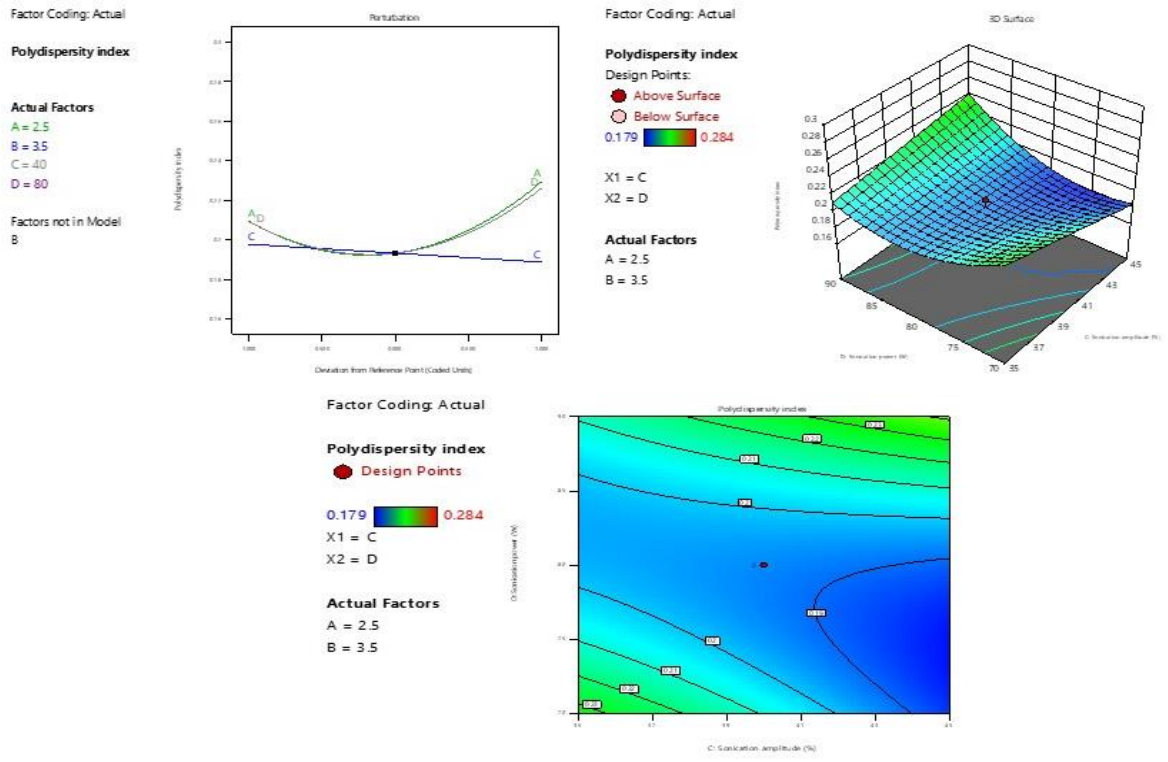

Fig. 3: Two-dimensional perturbation, 3D-RSM and contour plot– effect of A, B, C and D on PDI

Optimization process

We used Derringer's desirability approach to optimize response parameter-influencing process factors. Y_{max} and Y_{min} were used as objective functions (D) to convert all responses into desirability scales. A domain-wide grid search and feasibility analysis combined individual desire functions into a geometric mean. This was made easier with Design-Expert.

The best settings for maximum desirability were A: 2.41 cm, B: 3.61 min, C: 44.42 %, and D: 77.35 W, resulting in a D rating of 0.920, very good. The optimized conditions are shown in table 6. Fig. 4 shows the prediction model. These optimal conditions were used to prepare three batches of nanobubbles to test the model. Remarkably, the anticipated values and experimental results matched (fig. 4). The CCD and Derringer's desirability technique worked well to optimize entrectinib nanobubble composition.

Table 6: Optimum conditions attained by applying restrictions on response parameters

Independent variables	Optimized values	Predicted values		Actual values		
		Y1 (nm)	Y2	Batch	Y1 (nm)	Y2
A: Sonication distance	2.41 cm	84.17	0.183	B1	82.36±3.12	0.184±0.0005
B: Sonication time	3.61 min			B2	73.53±3.08	0.196±0.0005
C: Sonication amplitude	44.42 %			B3	87.18±2.28	0.178±0.0005
D: Sonication power	77.35 W					

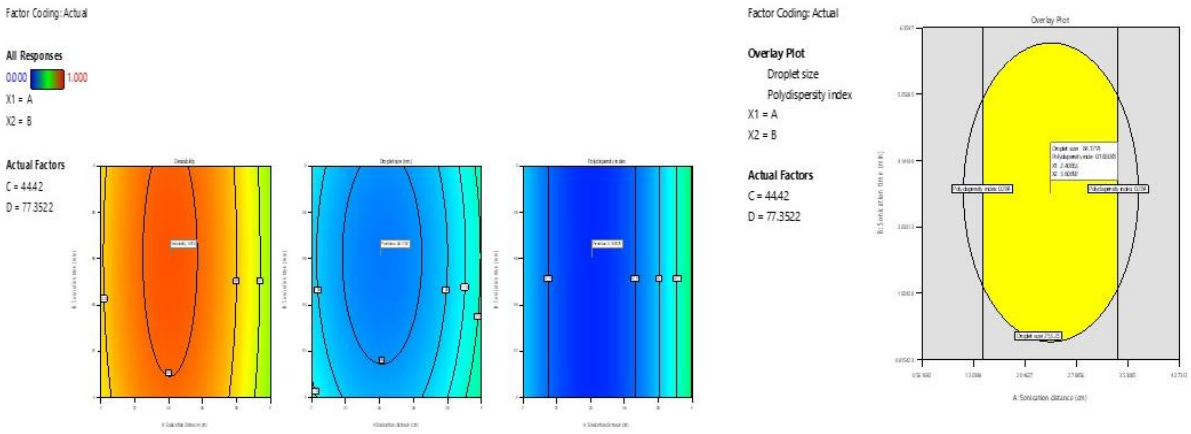

Fig. 4: Contour and overlay plots showing the global desirability value with point prediction

Characterization of nanobubble formulations

Entrectinib nanobubbles had consistent PS and low PDI across batches. High ZP indicated nanobubble storage stability. The average PS, PDI, and ZP of blank and entrectinib-loaded nanobubbles are shown in table 7. PS and PDI did not differ between blank and drug-loaded nanobubbles. TEM analyzed nanobubble morphology. The surface shape and core-shell structure of 70-90 nm nanobubbles were revealed by TEM images (fig. 5). Enterctinib was loaded into nanobubbles with 82.12% EE and 29.27% loading capacity. Entrectinib-loaded nanobubble aqueous suspension had a viscosity of 6.2 centipoises, acceptable for parenteral administration. Entrectinib loading into nanobubbles did not influence formulation viscosity.

Table 7: Physical characteristics of nanobubbles

Physical characteristics	Blank nanobubbles	Entrectinib loaded nanobubbles
Average PS	83.82± 3.29	73.53±3.08
PDI	0.178±0.005	0.196±0.005
ZP	-26.7±2.66	-25.3 ±2.98
EE	-	82.12±2.87
Loading capacity	-	29.27± 1.54

All the values were expressed in mean±SD (n=3).

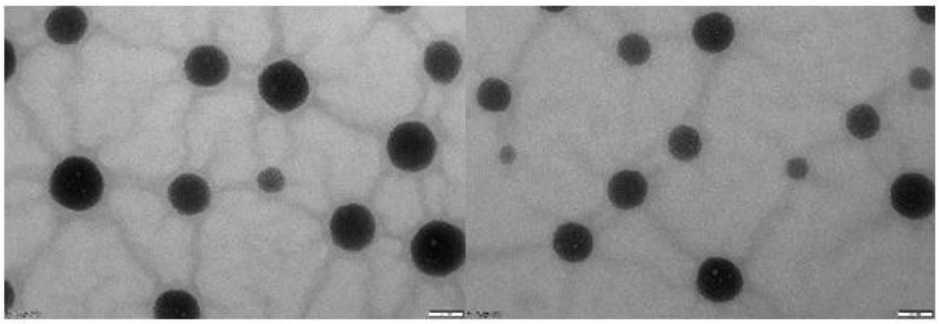

Fig. 5: TEM image of blank and entrectinib-loaded nanobubbles at 25,000× magnification

Spectral analysis and thermal behaviour

In fig. 6, entrectinib, PLGA, PVA, blank nanobubbles, and entrectinib-loaded nanobubbles are compared by FTIR. The entrectinib FTIR spectra showed peaks at 3430, 3313, 2945, 2865, 1606, and 1573 cm^{-1}. However, PLGA polymer gave distinctive peaks at 2998, 2948, 1454, 1426, and 1397 cm^{-1}. In its FTIR spectrum, PVA had prominent peaks at 3280, 2917, 1690, 1425, 1324, 1081, and 839 cm^{-1}. PLGA and PVA with vibrations were detected in blank nanobubble FTIR spectra. Entrectinib-loaded nanobubbles' FTIR spectra did not show the drug's distinctive peaks, suggesting entrapment in the PLGA matrix. Fig. 6 also shows the entrectinib-loaded PLGA nanobubble DSC thermogram. The DSC curve of pure entrectinib showed an endothermic peak at 200.32 °C, its melting point. PLGA's amorphous thermogram showed no melting point. A large endothermic peak at 369.4 °C suggested polymer heat degradation. A large endothermic peak at 212.6 °C suggested PVA melting, while a smaller hump at 40–42.5 °C may represent the glass transition temperature. Both blank and drug-loaded nanobubbles had similar melting transition parameters, suggesting that PLGA and PVA were unaffected by encapsulation. The absence of a crystalline drug material's prominent peak in the DSC study suggested the drug was imprisoned in the PLGA matrix. The thermogram's absence of the drug's endothermic peak supported this indication.

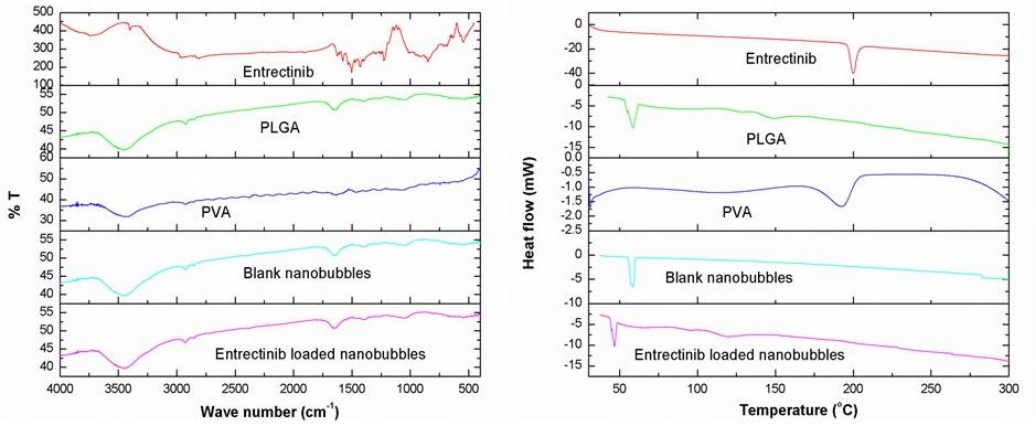

Fig. 6: FTIR spectra of entrectinib, PLGA, PVA, blank nanobubbles, and entrectinib loaded nanobubbles

Fig. 7 depicts entrectinib's *in vitro* release from nanobubbles in pH 7.4 phosphate buffer. This study examined how ultrasonic treatment affected nanobubble medication release and comparing nanobubble and entrectinib suspension medication release. The entrectinib suspension released less medication than the nanobubbles. Ultrasound-assisted medication release differed significantly from unassisted. After 6 h, sonication released 46.98% of entrectinib, while 26.42 % was released without. Ultrasound released 99.34% of entrectinib over 24 h, compared to 58.93% without. Ultrasound greatly promoted entrectinib release from nanobubbles. Ultrasound-induced microbubble creation and collapse cause cavitations, which generates localized high temperatures and pressures. Disrupting nanobubbles may enhance medication release. Ultrasound appears to promote medication release from nanobubble-based formulations, which could improve therapeutic effects. This cavitation effect's mechanisms and medication delivery implications could be studied.

Drug release order and mechanism were determined by fitting optimized nanobubble formulation drug release data into kinetic equations. R^2 assesses how well the model matches experimental data. Fitting R^2 values near 1 are better. Higuchi's square root of time model has the greatest R^2 value (0.9960), indicating a Good Fit and showing drug release follows a diffusion-based process. High R^2 scores for Zero Order (0.9235) and First Order (0.8951) models indicate a strong fit. Note that the First Order model has a negative "n" value, which is rare and may imply that it cannot effectively describe release kinetics. Korsmeyer-Peppas model fits well (R^2 = 0.9501), and the high "n" value (60.36) suggests a complex release mechanism due to non-Fickian or anomalous diffusion. In conclusion, the Higuchi model best describes this formulation's drug release kinetics, followed by Korsmeyer-Peppas. These findings shed light on the release process and can help optimize medication release from this formulation. Because the drug can be released at the specific target site instead of circulating throughout the body it will be more effective for a particular given dosage [28].

Ultrasound at different temperatures assessed entrectinib-loaded nanobubble stability. Sonication at 2.5 MHz for 5 min at 25 °C did not modify nanobubble morphology or structure. At 37 °C, nanobubbles subsided after 2 min of sonication and disappeared after 5 min, indicating destabilization. Because of its low boiling point, perfluoropentane turns into a gas at 37 °C. Small nanobubbles may change this transition temperature. Acoustic droplet generation occurs when ultrasound causes the gas core to go from nanodroplet to bubble. Entrectinib nanobubbles were stored at 4 °C, 25 °C, and 40 °C for 6 mo. Table 8 shows entrectinib nanobubble drug concentration, EE, and PS data at 0, 15, 30, 60, 120, and 180 days. Drug content was unaffected between 4 and 25 °C. Nanobubbles protected entrectinib from degradation at usual storage temperatures, as EE remained steady, especially at 4 and 25 °C. At 40 °C, EE decreased, suggesting nanobubble structural breakdown due to rising temperature. Drug-loaded nanobubbles had PDI values<0.2 during the stability testing. A constant and homogenous size distribution throughout the formulation confirmed its stability and appropriateness for prospective applications. A parenteral formulation must be safe. Hemolytic activity was measured to determine the safety of blank and entrectinib-loaded nanobubbles. PLGA nanobubble aqueous solutions were tested for hemolysis. We found that these nanobubbles were non-hemolytic even at 15 mg/ml. This suggests that blank nanobubbles do not harm red blood cells, bolstering their safety for application. When tested for hemolytic action, drug-loaded nanobubbles showed good safety for erythrocytes. This confirms the formulation's non-toxicity and parenteral safety.

***In vitro* cellular uptake study**

Entrectinib nanobubble uptake was examined in MCF-7 cells, a common breast cancer cell line. Measurements of fluorescence intensity were used. MCF-7 cells were incubated for 2 h to measure fluorescence intensity. The mean fluorescence intensity of cells treated with entrectinib nanobubbles with ultrasound was 8.58. This intensity was about 2 times higher than in cells treated with entrectinib nanobubbles alone, demonstrating that ultrasound enhances cellular absorption. Ultrasound can increase drug delivery, such as entrectinib cellular uptake, which could improve breast cancer therapy outcomes.

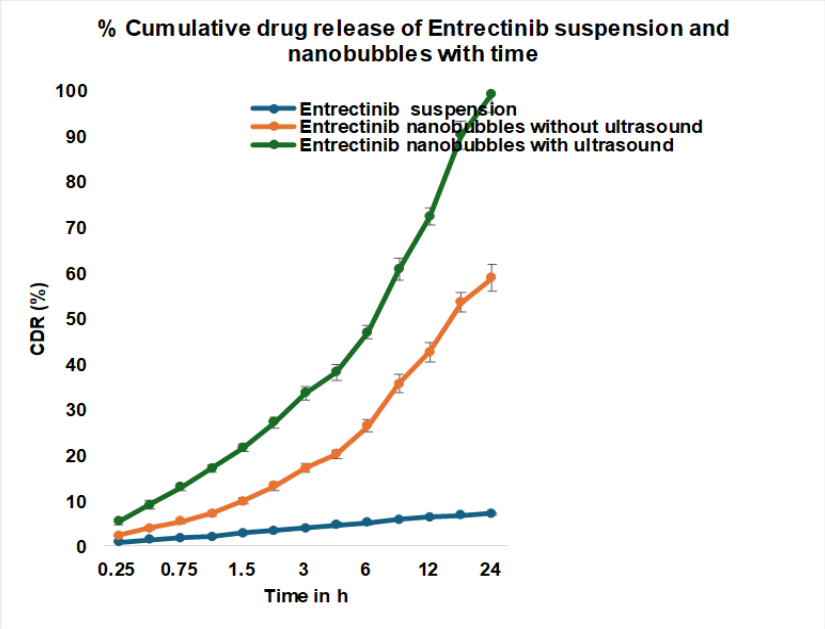

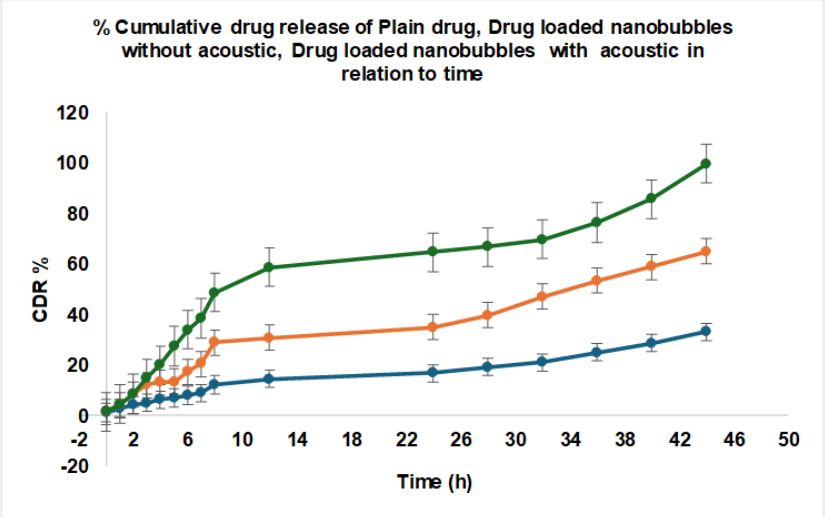

Fig. 7: *In vitro* drug release pattern with and without ultrasound assistance, all the values were expressed in mean±SD (n=3)

Table 8: EE, PS, and PDI of entrectinib nanobubbles stored at different temperatures

Temperature (°C)	Time (d)	PS (nm)	PDI	EE (%)
4±1 °C	0	73.53±3.08	0.196±0.005	82.12±2.87
	15	76.18±3.12	0.178± 0.005	80.78± 1.93
	30	69.32± 2.12	0.184± 0.005	84.82± 2.37
	60	70.67± 3.08	0.186±0.005	84.56± 3.12
	120	71.88± 2.13	0.178± 0.005	84.18± 4.08
	180	74.58± 1.98	0.182± 0.005	83.78± 3.05
25±2 °C	0	73.53±3.08	0.196±0.005	82.12±2.87
	15	70.98±2.89	0.188± 0.005	86.12± 2.76
	30	78.96±3.21	0.174± 0.005	86.28±3.37
	60	69.98± 2.88	0.162± 0.005	85.67± 3.87
	120	70.98±3.12	0.183±0.005	84.78± 4.12
	180	72.38±3.76	0.179± 0.005	84.12± 3.27
40±2 °C	0	73.53±3.08	0.196±0.005	82.12±2.87
	15	78.53±2.59	0.177± 0.005	78.73± 2.28
	30	88.12±3.38	0.185± 0.005	72.83± 4.02
	60	95.16±1.96	0.203± 0.005	67.62± 2.78
	120	108.98±2.87	0.215± 0.005	62.25± 2.26
	180	123.53±3.76	0.226± 0.005	58.78± 3.12

All the values were expressed in mean±SD (n=3)

***In vitro* cytotoxicity study**

The cytotoxicity of entrectinib-loaded nanobubbles against MCF-7 cells was assessed using the MTT assay, a common cell viability and cytotoxicity test. MCF-7 cells were tested for viability after exposure to entrectinib formulations at doses from 10 to 120 µM. All entrectinib formulations showed over 98% cell viability at 10 µM dosages, indicating negligible cytotoxicity. Cell viability continued to exceed 80% at a concentration of 20 µM. Possibly because this concentration is below the minimum effective concentration needed for substantial cytotoxicity. Nanobubbles with ultrasound had the lowest cell viability as concentration rose [34]. At 50% cell inhibition, IC50 values were determined. Free entrectinib showed an IC50 of 69.89 µM, while nanobubbles with and without ultrasound had IC50 values of 38.13 and 31.27 µM, respectively. It appears that ultrasound-assisted nanobubbles released entrectinib into cells with high sensitivity and potential for cytotoxicity. The results suggest that this formulation may improve MCF-7 cell treatment outcomes, an important breast cancer treatment concern. Results of Cellular uptake and *in vitro* cytotoxicity of plain entrectininb, entrectininb nanobubbles without ultrasound, and entrectininb nanobubbles with ultrasound are shown in fig. 8 (A and B). Due to slow release of drug from the nanobubbles, at the proposed concentration, the amount of free drug in nanibubbles was much lower than that of comparator. Thus, the improved cytotoxic effect on the cancer cell lines may be due to higher cell penetration of the nanobubbles [3].

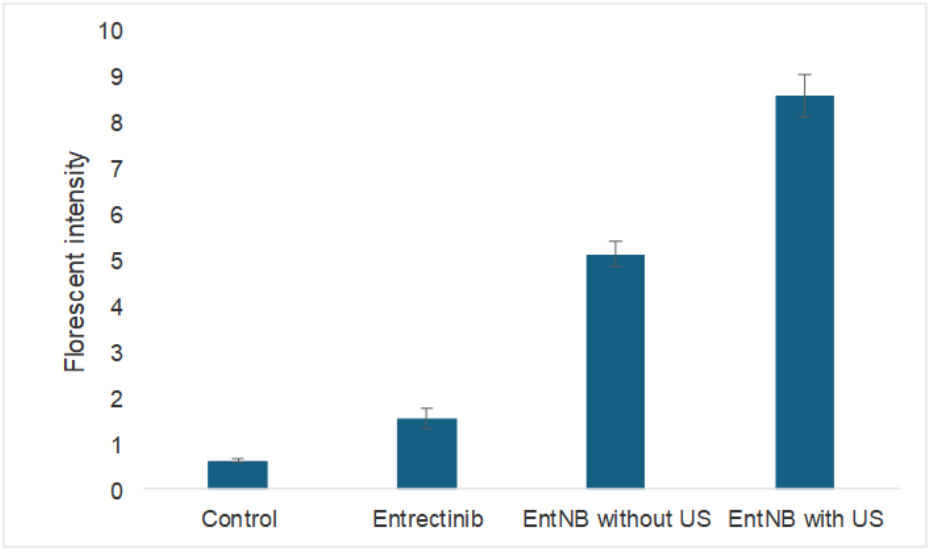

(A)

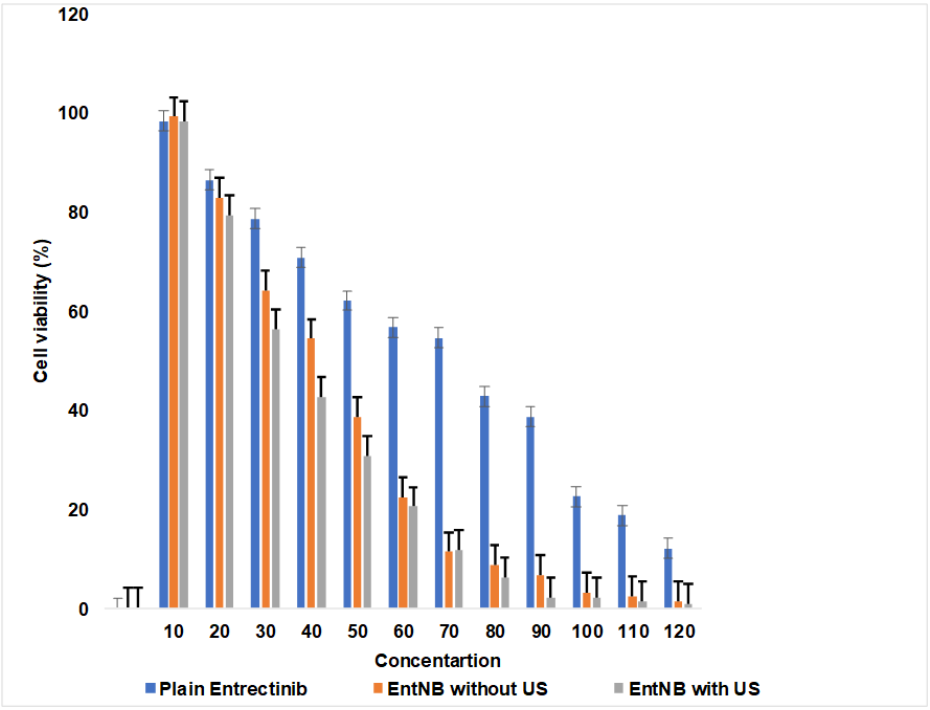

(B)

Fig. 8: Results of cellular uptake and *in vitro* cytotoxicity of plain entrectininb, entrectininb nanobubbles without ultrasound, and entrectininb nanobubbles with ultrasound; all the values were expressed in mean±SD (n=3)

CONCLUSION

Our goal was to create nanobubbles with a PLGA shell and a perfluoropentane core to deliver entrectinib. We optimized formulation components using the response surface approach to produce an optimal PS and homogeneous size distribution. The nanobubbles' PS was extremely consistent under these optimized settings. Thus, entrectinib solubility is critical to medication efficacy, according to our data. Entrectinib was more soluble in nanobubbles than in suspension, especially at different pH levels. Enhanced solubility may improve medicinal efficacy and bioavailability. Our *in vitro* dissolution studies confirmed entrectinib nanobubbles' benefits. We also examined entrectinib nanobubbles' therapeutic potential *in vitro*. Nanobubbles inhibited tumor cell proliferation better, suggesting promising results. This highlights the promise of PLGA nanobubbles in ultrasound-responsive formulations for targeted medication delivery in cancer and other disorders. Overall, entrectinib-loaded PLGA-shelled nanobubbles could revolutionize medication delivery. Improved solubility, dissolution characteristics, bioavailability, and therapeutic efficacy show nanobubble-based drug delivery systems' potential future in oncology and beyond.

FUNDING

Nil

AUTHORS CONTRIBUTIONS

The research work and writing were completed by N. P. and reviewed and edited by D. V. R. N. B. Both authors agree with the submission and publication. Both have read and agreed to the published edition of the manuscript.

CONFLICT OF INTERESTS

There are no known, potential, or perceived conflicts of interest on the part of the writers of this work.

REFERENCES

1. Frampton JE. Entrectinib: a review in NTRK+ solid tumours and ROS1+ NSCLC. Drugs. 2021 Apr;81(6):697-708. doi: 10.1007/s40265-021-01503-3, PMID 33871816.
2. Pravallika KE, Prameela RA, Ratna KM. Bioanalytical method development and validation of entrectinib in rat plasma by liquid chromatography-tandem mass spectrometry. Asian J Pharm Clin Res. 2020 Nov;13(11):155-63. doi: 10.22159/ajpcr.2020.v13i11.39005.
3. Palanati M, Bhikshapathi DV. Determination of *in vitro* cytotoxicity of entrectinib and pemigatinib nanosponges tablets on a 498 mcf-7 and panc-1 cell line. Int J Pharm Pharm Sci. 2024 Feb;16(2):12-6. doi: 10.22159/ijpps.2024v16i2.49567.
4. Rolfo C, Ruiz R, Giovannetti E, Gil Bazo I, Russo A, Passiglia F. Entrectinib: a potent new TRK ROS1 and ALK inhibitor. Expert Opin Investig Drugs. 2015 Nov;24(11):1493-500. doi: 10.1517/13543784.2015.1096344, PMID 26457764.
5. Meneses Lorente G, Bentley D, Guerini E, Kowalski K, Chow Maneval E, YU L. Characterization of the pharmacokinetics of entrectinib and its active M5 metabolite in healthy volunteers and patients with solid tumors. Invest New Drugs. 2021 Jun;39(3):803-11. doi: 10.1007/s10637-020-01047-5, PMID 33462752.
6. DE Braud FG, Niger M, Damian S, Bardazza B, Martinetti A, Pelosi G. Alka-372-001: First in human phase I study of entrectinib an oral pan TRK ROS1 and ALK inhibitor in patients with advanced solid tumors with relevant molecular alterations. J Clin Oncol. 2015;33 Suppl 15:2517. doi: 10.1200/jco.2015.33.15_suppl.2517.
7. Al Salama ZT, Keam SJ. Entrectinib: first global approval. Drugs. 2019 Sep;79(13):1477-83. doi: 10.1007/s40265-019-01177-y, PMID 31372957.
8. Parrott N, Stillhart C, Lindenberg M, Wagner B, Kowalski K, Guerini E. Physiologically based absorption modelling to explore the impact of food and gastric pH changes on the pharmacokinetics of entrectinib. AAPS J. 2020 May;22(4):78. doi: 10.1208/s12248-020-00463-y, PMID 32458089.
9. Liu D, Offin M, Harnicar S, LI BT, Drilon A. Entrectinib: an orally available selective tyrosine kinase inhibitor for the treatment of NTRK ROS1 and ALK fusion-positive solid tumors. Ther Clin Risk Manag. 2018 Jul;14:1247-52. doi: 10.2147/TCRM.S147381, PMID 30050303.
10. Wang Q, Fang P, Zheng L, YE L. Quantification and pharmacokinetic study of entrectinib in rat plasma using ultra-performance liquid chromatography-tandem mass spectrometry. Biomed Chromatogr. 2019 Apr;33(4):e4467. doi: 10.1002/bmc.4467, PMID 30549079.
11. Doebele RC, Drilon A, Paz Ares L, Siena S, Shaw AT, Farago AF. Entrectinib in patients with advanced or metastatic NTRK fusion-positive solid tumours: integrated analysis of three phase 1-2 trials. Lancet Oncol. 2020 Feb;21(2):271-82. doi: 10.1016/S1470-2045(19)30691-6, PMID 31838007.
12. Wen H, Jung H, LI X. Drug delivery approaches in addressing clinical pharmacology related issues: opportunities and challenges. AAPS J. 2015 Nov;17(6):1327-40. doi: 10.1208/s12248-015-9814-9, PMID 26276218.
13. Kumari L, Choudhari Y, Patel P, Gupta GD, Singh D, Rosenholm JM. Advancement in solubilization approaches: a step towards bioavailability enhancement of poorly soluble drugs. Life (Basel). 2023 Apr;13(5):1099. doi: 10.3390/life13051099, PMID 37240744.
14. YU YQ, Yang X, WU XF, Fan YB. Enhancing permeation of drug molecules across the skin via delivery in nanocarriers: novel strategies for effective transdermal applications. Front Bioeng Biotechnol. 2021 Mar;9:646554. doi: 10.3389/fbioe.2021.646554, PMID 33855015.
15. Patra JK, Das G, Fraceto LF, Campos EV, Rodriguez Torres MD, Acosta Torres LS. Nano-based drug delivery systems: recent developments and future prospects. J Nanobiotechnology. 2018 Jan;16(1):71. doi: 10.1186/s12951-018-0392-8, PMID 30231877.
16. SS, SA, Krishnamoorthy K, Rajappan M. Nanosponges: a novel class of drug delivery system review. J Pharm Pharm Sci. 2012 Jan;15(1):103-11. doi: 10.18433/j3k308, PMID 22365092.
17. Foroughi Nia B, Barar J, Memar MY, Aghanejad A, Davaran S. Progresses in polymeric nanoparticles for delivery of tyrosine kinase inhibitors. Life Sci. 2021 Aug;278:119642. doi: 10.1016/j.lfs.2021.119642, PMID 34033837.
18. Jin J, Yang L, Chen F, GU N. Drug delivery system based on nanobubbles. Interdisciplinary Materials. 2022 Apr;1(4):471-94. doi: 10.1002/idm2.12050.
19. Pasupathy R, Pandian P, Selvamuthukumar S. Nanobubbles: a novel targeted drug delivery system. Braz J Pharm Sci. 2022 Dec;58. doi: 10.1590/s2175-97902022e19604.
20. Ponnaganti M, Ancha KB, Palanati M. Formulation and optimization of ceritinib loaded nanobubbles by box behnken design. Int J Appl Pharm. 2022 Apr;14(4):219-26.
21. Jin J, Yang L, Chen F, GU N. Drug delivery system based on nanobubbles. Interdisciplinary Materials. 2022 Apr;1(4):471-94. doi: 10.1002/idm2.12050.
22. Gao J, Liu J, Meng Z, LI Y, Hong Y, Wang L. Ultrasound assisted C3F8 filled PLGA nanobubbles for enhanced FGF21 delivery and improved prophylactic treatment of diabetic cardiomyopathy. Acta Biomater. 2021 Aug;130:395-408. doi: 10.1016/j.actbio.2021.06.015.
23. Jayita D, Anima D, Lalhlenmawia H. Formulation and in vitro evaluation of poly(d, l-lactide-co-glycolide) (PLGA) nanoparticles of ellagic acid and its effect on human breast cancer mcf-7 cell line. Int J Curr Pharm Res. 2021 May;13(5):56-62.
24. SU C, Ren X, Nie F, LI T, LV W, LI H. Current advances in ultrasound combined nanobubbles for cancer targeted therapy: a review of the current status and future perspectives. RSC Adv. 2021 Apr;11(21):12915-28. doi: 10.1039/d0ra08727k, PMID 35423829.
25. Hema AN, Gaayathri G, Gundeti S. Development of orodispersible tablets of loratadine containing an amorphous solid dispersion of the drug in soluplus® using design of experiments. Int J Pharm Pharm Sci. 2023 Aug;15(8):19-27.
26. Rampado R, Peer D. Design of experiments in the optimization of nanoparticle-based drug delivery systems. J Control Release. 2023 Jun;358:398-419. doi: 10.1016/j.jconrel.2023.05.001, PMID 37164240.
27. Iqbal M, Zafar N, Fessi H, Elaissari A. Double emulsion solvent evaporation techniques used for drug encapsulation. Int J

Pharm. 2015 Feb;496(2):173-90. doi: 10.1016/j.ijpharm.2015.10.057, PMID 26522982.
28. Candioti LV, DE Zan MM, Camara MS, Goicoechea HC. Experimental design and multiple response optimization using the desirability function in analytical methods development. Talanta. 2014 Jun;124:123-38. doi: 10.1016/j.talanta.2014.01.034, PMID 24767454.
29. Kumar V, Bhalla A, Rathore AS. Design of experiments applications in bioprocessing: concepts and approach. Biotechnol Prog. 2014 Jan;30(1):86-99. doi: 10.1002/btpr.1821, PMID 24123959.
30. Paterakis NG, Gibescu M, Bakirtzis AG, Catalao JP. A multi-objective optimization approach to risk-constrained energy and reserve procurement using demand response. IEEE Trans Power Syst. 2017 Apr;33(4):3940-54. doi: 10.1109/TPWRS.2017.2785266.
31. Zhang X, Zheng Y, Wang Z, Huang S, Chen Y, Jiang W. Methotrexate loaded PLGA nanobubbles for ultrasound imaging and synergistic targeted therapy of residual tumor during HIFU ablation. Biomaterials. 2014 Jun;35(19):5148-61. doi: 10.1016/j.biomaterials.2014.02.036, PMID 24680663.
32. Yedgar S, Barshtein G, Gural A. Hemolytic activity of nanoparticles as a marker of their hemocompatibility. Micromachines. 2022 Dec;13(12):2091. doi: 10.3390/mi13122091, PMID 36557391.
33. Wang S, Liu X, Chen S, Liu Z, Zhang X, Liang XJ. Regulation of Ca2+ signaling for drug-resistant breast cancer therapy with mesoporous silica nanocapsule encapsulated doxorubicin/sirna cocktail. ACS Nano. 2019;13(1):274-83. doi: 10.1021/acsnano.8b05639, PMID 30566319.
37. Zhang X, Zheng Y, Wang Z, Huang S, Chen Y, Jiang W. Methotrexate loaded PLGA nanobubbles for ultrasound imaging and synergistic targeted therapy of residual tumor during HIFU ablation. Biomaterials. 2014 Jun;35(19):5148-61. doi: 10.1016/j.biomaterials.2014.02.036, PMID 24680663.
38. XU JS, Huang J, Qin R, Hinkle GH, Povoski SP, Martin EW. Synthesizing and binding dual mode poly (lactic-co-glycolic acid) (PLGA) nanobubbles for cancer targeting and imaging. Biomaterials. 2010 Jul;31(7):1716-22. doi: 10.1016/j.biomaterials.2009.11.052, PMID 20006382.
39. Yan Y, Chen Y, Liu Z, Cai F, Niu W, Song L. Brain delivery of curcumin through low-intensity ultrasound-induced blood-brain barrier opening via lipid-PLGA nanobubbles. Int J Nanomedicine. 2021 Nov;16:7433-47. doi: 10.2147/IJN.S327737, PMID 34764649.
40. Brzezinska R, Wirkowska Wojdyla M, Piasecka I, Gorska A. Application of response surface methodology to optimize the extraction process of bioactive compounds obtained from coffee silverskin. Appl Sci. 2023 Apr;13(9):5388. doi: 10.3390/app13095388.
41. Danaei M, Dehghankhold M, Ataei S, Hasanzadeh Davarani F, Javanmard R, Dokhani A. Impact of particle size and polydispersity index on the clinical applications of lipidic nanocarrier systems. Pharmaceutics. 2018 May;10(2):57. doi: 10.3390/pharmaceutics10020057, PMID 29783687.